Proton occupation numbers in ^{206}Pb from the ($\vec{d}$,^{3}He) reaction

M. C. Radhakrishna,* N. G. Puttaswamy,* H. Nann, J. D. Brown,† W. W. Jacobs, W. P. Jones, D. W. Miller, P. P. Singh, and E. J. Stephenson

Department of Physics and Indiana University Cyclotron Facility, Indiana University, Bloomington, Indiana 47405

(Received 17 August 1987)

Angular distributions of the differential cross section and vector analyzing power have been measured for the ^{206}Pb($\vec{d}$,^{3}He)^{205}Tl reaction at an incident deuteron energy of 79.4 MeV. Spin-parity assignments have been made for seventeen transitions to residual nuclear states up to 2.8 MeV in excitation. Optical-model parameters have been obtained for both the entrance and exit channels by fitting elastic scattering data measured to large angles. Exact finite-range distorted-wave Born-approximation calculations have been performed and spectroscopic strengths have been deduced for all the observed transitions. The proton occupation numbers in ^{206}Pb for $3s_{1/2}$, $2d_{3/2}$, $2d_{5/2}$, and $1h_{11/2}$ orbitals indicate a general depletion of about 30%, to be compared to 18% depletion previously reported in ^{208}Pb. The $3s_{1/2}$ proton occupation number in ^{206}Pb deduced from this experiment is in good agreement with the results of recent (e,e'p) experiments.

I. INTRODUCTION

Over the course of the last few years, the structure of nuclei in the lead region has received considerable attention by both theorists and experimentalists. The charge density difference $\Delta\rho(r)$ between ^{206}Pb and ^{205}Tl, as measured by elastic electron scattering,[1,2] clearly exhibits the characteristic shape of the $3s_{1/2}$ wave function, providing strong evidence for the nucleonic picture of nuclei at nuclear matter densities. From a comparison with the predictions from the mean-field theory, a value for the difference between the $3s_{1/2}$ proton occupation numbers in ^{206}Pb and ^{205}Tl has been deduced as

$$z = n(206) - n(205) = 0.7 \pm 0.1 \ . \quad (1)$$

This result has been interpreted as evidence for a 30% depletion (quenching) of the single-particle $3s_{1/2}$ strength. Theoretical calculations[3-5] for the doubly magic nucleus ^{208}Pb also predict a depletion of the shell-model orbitals of up to 30%. Recently, (e,e'p) measurements[6,7] and (d,^{3}He) studies at $E = 52$ MeV (Refs. 8 and 9) have been carried out. The occupation numbers for the $3s_{1/2}$ orbital in ^{208}Pb, ^{206}Pb, and ^{205}Tl were extracted using the value of $z = 0.7$ together with accurate relative transition strengths; a depletion of (18 ± 9)% was found for ^{208}Pb.

In this paper we present a study of the ^{206}Pb($\vec{d}$,^{3}He)^{205}Tl reaction at $E_d = 79.4$ MeV in which we deduce the proton occupation numbers for all orbitals close to the Fermi surface of ^{206}Pb. The optical-model parameters needed to generate the distorted waves for the exact finite-range distorted-wave Born-approximation (DWBA) calculations have been obtained from elastic-scattering measurements, for both entrance and exit channels, at the appropriate center-of-mass energies for the ($\vec{d}$,^{3}He) data. Spectroscopic factors were deduced for 17 transitions, allowing proton occupation numbers to be extracted, in particular for the $3s_{1/2}$, $2d_{3/2}$, $2d_{5/2}$, and $1h_{11/2}$ orbitals.

The biggest uncertainty in the spectroscopic strength extracted from transfer-reaction data generally arises from the prescription of the radial form factor in the DWBA calculations. In the most commonly used well-depth (WD) method, for a given choice of geometric parameters (radius r_0 and diffuseness a_0), the depth of a volume Woods-Saxon potential is adjusted to reproduce the separation energy of the particle to be transferred from the specified orbital; this method is expected to yield reasonable results for nuclei near closed shells. An alternate method has been suggested by Austern[10] and Rae,[11] wherein the transferred nucleon is bound in a fixed mean-field potential plus an additional surface-peaked potential, the depth of the latter being adjusted to reproduce the separation energy of the transferred particle, thus guaranteeing the correct shape in the tail region of the radial form factor. This surface-peak (SP) method has been applied by Winfield *et al.*[12] to a study of the (^{9}Be,^{10}B) reaction on light nuclei. In the present paper we study the sensitivity of the spectroscopic strengths derived from the ($\vec{d}$,^{3}He) reaction with respect to both the WD and SP methods. In addition, the root-mean-square (rms) radii of the individual proton orbitals in ^{206}Pb (which depend sensitivitely on the geometry of the bound-state potential) are compared with predictions from Hartree-Fock calculations.[13,14]

Proton pickup from ^{206}Pb has also been studied previously through the (t,α) reaction at $E_t = 13.5$ MeV (Ref. 15) and $E_t = 17$ MeV (Ref. 16). Proton stripping on ^{205}Tl has been measured through the reaction ^{205}Tl(α,t)^{206}Pb (g.s.) at energies from $E_\alpha = 20$ to 25 MeV in order to determine the normalization constant for (α,t) reactions.[17] Information concerning the energy levels of ^{205}Tl has been summarized by Schmorak.[18]

The experimental procedures used in the present in-

vestigation are described in Sec. II, while the analyses carried out to obtain the best fit optical-model parameters are illustrated in Sec. III. Distorted-wave analyses employing exact finite-range DWBA calculations are reviewed in Sec. IV, and a discussion of the results of the present study is presented in Sec. V.

II. EXPERIMENTAL PROCEDURE

The ^{206}Pb($\vec{d}$, ^{3}He)^{205}Tl reaction was studied using a 79.4-MeV vector-polarized deuteron beam at the Indiana University Cyclotron Facility. Angular distribution measurements of the differential cross section $\sigma(\theta)$ and vector analyzing power $A_y(\theta)$ were made. The outgoing ^{3}He particles were detected between laboratory angles (θ_{lab}) of 6° and 20°, in 2° intervals, and between 20° and 32°, in 3° intervals. In order to obtain optical-model parameters required for the DWBA calculations, the following elastic scattering measurements were made: (i) $\sigma(\theta)$ and $A_y(\theta)$ for deuterons on ^{206}Pb at 79.4 MeV, and (ii) $\sigma(\theta)$ for ^{3}He on ^{205}Tl at 78.4 MeV. The elastically scattered deuterons from ^{206}Pb were detected between θ_{lab} of 13° and 50° in 1° steps, and between 50° and 130° in 2°, 3°, or 4° steps. ^{3}He particles scattered from ^{205}Tl were observed between θ_{lab} of 9° and 50° in steps of 1°, and between 50° and 76° in steps of 2°. The energy of ^{3}He particles scattered from ^{205}Tl was chosen to match the center-of-mass energy for the time-reversed reaction, taking into account the reaction Q value.

An atomic beam source[19] was used to generate the polarized deuteron beam for these measurements. Analyzing-power measurements were made by periodically changing the spin state (about twice per minute) during data acquisition. The deuteron polarization was measured frequently by inserting a target gas cell containing ^{3}He gas into the beam line between the injector and the main-stage cyclotrons. Details of the polarization measurements are discussed in Ref. 20. The "up" and "down" polarizations of the beam were observed to remain nearly constant, with values for the two spin orientations of around $+0.58$ and -0.60; the actual values used for computing the analyzing powers in the ^{206}Pb($\vec{d}$,^{3}He)^{205}Tl reaction and $\vec{d}$+ ^{206}Pb elastic scattering were determined by interpolation from polarizations measured periodically during the experiment. We assume that the polarization measured with the polarimeter between the two cyclotrons is maintained throughout the acceleration process in the main cyclotron and the subsequent beam transport system.

Beam energies were measured by deflection through a 42° energy analysis magnet and slit system, located in the high-energy beam line following the main cyclotron. The beam current was varied between 1 nA and about 200 nA, as determined by the rate at which events could be processed without incurring large dead times. The total flux was calculated from the integrated charge recorded in a beam-stopping Faraday cup located downstream of the target. At forward angles ($\theta_{lab} \leq 50°$), a split Faraday cup placed directly in the scattering chamber was used. The separate current signals from the left and right halves of this cup were used to center the beam on target during data acquisition. For large-angle measurements ($\theta_{lab} > 50°$), a heavily shielded beam dump located in the wall far behind the target chamber was used. The latter arrangement significantly decreased room background, enabling measurement of the small cross sections at large angles.

The target materials utilized were 99.8% isotopically enriched ^{206}Pb and 99.4% isotopically enriched ^{205}Tl. Self-supporting ^{206}Pb targets of thicknesses 11.5, 2.8, and 0.6 mg/cm^2 were used during the course of the experiment. The 11.5-mg/cm^2 target was made by rolling, and the 2.8 and 0.6 mg/cm^2 targets were made by vacuum evaporation. ^{205}Tl targets of thicknesses 1.70 and 1.29 mg/cm^2 were made by vacuum evaporation onto a 20 μg/cm^2 carbon backing after reduction in a hydrogen furnace. All $\vec{d}$+ ^{206}Pb cross sections were normalized to the value obtained with the 11.5-mg/cm^2 target, whose areal density was accurately determined by weighing, while the ^{3}He+ ^{205}Tl cross sections were normalized to the value obtained with the 1.70-mg/cm^2 target. Measurements of cross sections with the various targets were repeated at selected angles to check reproducibility.

Charged particles from the ($\vec{d}$,^{3}He) reaction and from elastic scattering were momentum analyzed by a quadrupole-dipole-dipole-multipole (QDDM) magnetic spectrometer. The spectrometer entrance slits were adjusted to provide solid angles between 0.8 and 1.5 msr; the larger values were used at large scattering angles. The corresponding angular acceptance varied from 1.15° to 1.72°. Focal-plane positions of the detected particles were measured with a helical proportional counter. The reaction products were identified on the basis of energy-loss signals from two plastic scintillation detectors mounted behind the helical counter. Dead-time corrections were determined by feeding pulser signals, triggered at a rate proportional to the beam current, into the helical counter and front end of the electronics system. The pulser signals were analyzed along with the data from real events. The typical overall energy resolution was about 60 keV.

The particle spectra were analyzed with the computer code ALLFIT.[21] A typical ^{3}He spectrum for the ^{206}Pb($\vec{d}$, ^{3}He)^{205}Tl reaction taken at $\theta_{lab}=8°$ is shown in Fig. 1. Peak areas were obtained by fitting the spectrum using a Gaussian peak shape whose parameters were obtained by fitting the shape of the peak corresponding to the first excited state of ^{205}Tl. Thus, both spin-up and spin-down spectra were analyzed with common peak shapes, helping to reduce systematic errors. The cross sections and analyzing powers were calculated from individual peak areas of the spin-up and spin-down spectra. The error bars shown in the angular distributions (Figs. 2–9) reflect only counting statistics, based upon between 20 and 1000 summed counts in a typical run. The $\theta_{lab}=6°$ cross sections have been adjusted upward by a factor of 1.6 as a result of the Faraday cup partially obscuring the entrance opening of the spectrometer at this most forward angle; an error of 15% has been assigned in this case.

Energy calibration for the spectra was carried out by fitting a quadratic polynomial to the ^{3}He momenta as a

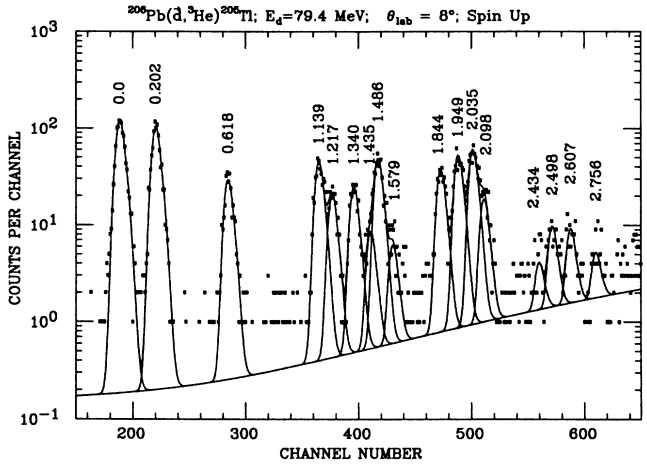

FIG. 1. Semilog plot of the ^{3}He energy spectrum, using one deuteron spin orientation, for the ^{206}Pb(d,^{3}He)^{205}Tl reaction at a bombarding energy of 79.4 MeV at $\theta_{lab}=8°$. The positions of peaks corresponding to states in ^{205}Tl are indicated by their excitation energies in MeV, and the solid curve indicates the fit to the spectrum obtained with the fitting procedure described in the text.

function of channel number. Relativistic kinematics were used. Table I lists the excitation energies for ^{205}Tl levels obtained from this experiment as well as the values determined from previous studies.

III. OPTICAL-MODEL ANALYSES

Differential cross section and analyzing power angular distributions of 79.4-MeV elastically scattered deuterons from ^{206}Pb are shown in Fig. 2. An optical-model prediction using the global optical-model parameter set of Daehnick *et al.*[22] for deuterons on ^{206}Pb is displayed as a dashed line (D0). Although oscillatory structures in the angular distributions for both the differential cross section $\sigma(\theta)$ and analyzing power $A_y(\theta)$ are similar to those observed in our data, this prediction nonetheless fails to reproduce the $\sigma(\theta)$ data at large angles, and severely underestimates $A_y(\theta)$ beyond 60° where it approaches its maximum possible value (see Fig. 2).

The differential cross section angular distribution for elastic scattering of 78.4-MeV ^{3}He from ^{205}Tl is shown in Fig. 3. The recent global parameters for ^{3}He on ^{205}Tl of Trost *et al.*[23] similarly do not correctly predict the

TABLE I. Energy levels of ^{205}Tl.

Present results		Nuclear data sheets[a]		^{206}Pb($\vec{t}$,α)^{205}Tl[b]		^{206}Pb(t,α)^{205}Tl[c]	
E_x (keV)	J^π	E_x (keV)	J^π	E_x (keV)	J^π	E_x (keV)	J^π
0	$\frac{1}{2}^+$	0[d]	$\frac{1}{2}^+$	0	$\frac{1}{2}^+$	0	$\frac{1}{2}^+$
202±5	$\frac{3}{2}^+$	203.75[d]	$\frac{3}{2}^+$	205±5	$\frac{3}{2}^+$	200	$\frac{3}{2}^+$
618±5	$\frac{5}{2}^+$	619.42[d]	$\frac{5}{2}^+$	614±5	$\frac{5}{2}^+$	620	$\frac{5}{2}^+$
1139±5	$\frac{3}{2}^+$	1140.75[d]	$\frac{3}{2}^+$	1138±5	$\frac{3}{2}^+$	1140	$(\frac{3}{2}^+)$
1217±5	$\frac{1}{2}^+$	1218.98	$\frac{1}{2}^+$	1222±5	$\frac{1}{2}^+$	1210	$\frac{1}{2}^+$
1340±5	$\frac{3}{2}^+$	1340.30[d]	$\frac{3}{2}^+$	1341±5	$\frac{3}{2}^+$	1340	
1435±10	$\frac{1}{2}^+$	1433.79	$(\frac{1}{2}^+)$	1436±5	$(\frac{1}{2}^+)$	1430	
1486±5	$\frac{11}{2}^-$	1484.05[d]	$\frac{11}{2}^-$	1491±5	$\frac{11}{2}^-$	1480	
		1574.03	$(\frac{3}{2}^+)$				
1579±15	$\frac{5}{2}^+$					1580	
1844±15	$\frac{5}{2}^+$	1866.4	$(\frac{5}{2}^+)$	1859±10	$\frac{5}{2}^+, \frac{11}{2}^-$	1860	
1949±5	$\frac{5}{2}^+$	1951[d]	$(\frac{5}{2}^+)$	1953±10	$\frac{5}{2}^+, \frac{11}{2}^-$	1960	
		2002.46	$(\frac{3}{2}^+)$				
2035±10	$\frac{5}{2}^+$			2044±10	$\frac{11}{2}^-, \frac{5}{2}^+$	2040	
		2098.22	$(\frac{1}{2}^+, \frac{3}{2}^+)$				
2098±10	$\frac{5}{2}^+$			2112±10	$\frac{11}{2}^-, \frac{5}{2}^+$	2120	
2434±15	$\frac{5}{2}^+$			2420±10		2430	
		2488.48	$(\frac{5}{2})^-$				
2498±15	$\frac{11}{2}^-$			2482±10		2490	
		2623.08	$(\frac{5}{2})^-$				
2607±15	$\frac{11}{2}^-$			2588±10	$\frac{5}{2}^+, \frac{11}{2}^-$	2600	
		2750.6	$(\frac{1}{2}^+, \frac{3}{2}^+)$	2714±10		2740	
2756±15	$\frac{5}{2}^+$						

[a]Reference 18.
[b]Reference 16.
[c]Reference 15.
[d]Energy level values used for the present calibration.

shape and magnitude of $\sigma(\theta)$ between 30° and 80° (see dashed curve). We have therefore systematically analyzed the elastic-scattering data from the present investigation in the conventional framework of the optical model in order to search for parameters which would more adequately describe the data.

A. Optical potential

The data analyses were performed with a 13-parameter optical model consisting of complex central and spin-orbit potentials; the automatic search code GOMFIL developed by Leeb[24] was used. The complex potential was of the form

$$V(r)=V_c(r)-V_R(1+e^{x/\alpha})^{-\alpha}-iW_s(1+e^{y/\beta})^{-\beta}$$
$$+i4W_D(d/dy)(1+e^{y/\beta})^{-\beta}$$
$$-2\left[\frac{\hbar}{m_\pi c}\right]^2[(V_{so}+iW_{so})f_{so}(r)](\boldsymbol{l}\cdot\mathbf{S}) \quad (2)$$

with

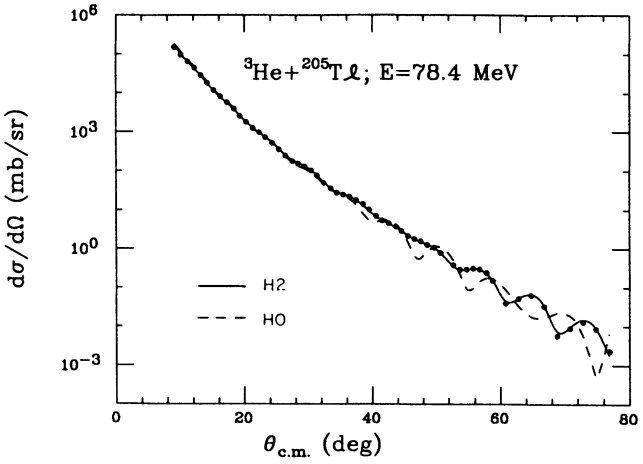

FIG. 3. Differential cross-section angular distributions for elastic scattering of 78.4 MeV ^{3}He from ^{205}Tl. The solid curve is the best fit obtained from set H2, and the dashed curve is the prediction obtained using global set H0, as described in the text.

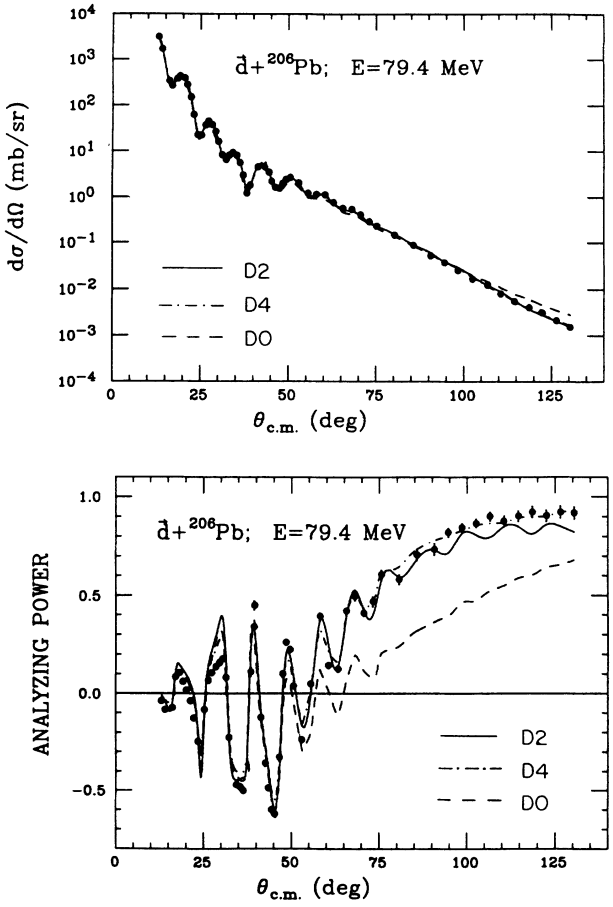

FIG. 2. Differential cross-section and analyzing-power angular distributions for elastic scattering of 79.4-MeV deuterons from ^{206}Pb. The curves represent different optical-model parametrizations as described in the text.

$$x=(r-r_0A^{1/3})/a_0\ ,$$
$$y=(r-r_wA^{1/3})/a_w\ .$$

The exponents α,β of the nuclear potential form factors can be chosen different from unity in order to modify the real or imaginary central potential, without changing the asymptotic fall off which remains as $\sim e^{-r/a}$; a Woods-Saxon (WS) form for $\alpha=1$, or a squared Woods-Saxon (WS^2) form for $\alpha=2$, were used in the present study.

The Coulomb potential has the form

$$V_c(r)=Z_pZ_Te^2[3-(r/R_c)^2]/(2R_c) \quad \text{for } r<R_c=r_cA^{1/3}$$
$$=Z_pZ_Te^2/r \quad \text{for } r>R_c\ . \quad (3)$$

The real and imaginary spin-orbit form factors were of the conventional Thomas type:

$$f_{so}(r)=(1/r)(d/dr)(1+e^s)^{-1}\ ,$$

with

$$s=(r-r_{so}A^{1/3})/a_{so} \quad (4)$$

where r_{so},a_{so} were chosen differently for V_{so},W_{so}.

In the fitting procedure, the influence of the cross-section data on the final results would have been much greater than that of the analyzing-power data, because of the smaller uncertainties in $\sigma(\theta)$ as compared to those in $A_y(\theta)$. Therefore, in the present analyses, the uncertainty for the differential cross-section data was taken as 2% for all angles for which the actual statistical error was less than 2%. On the other hand, a constant error of 1.5% was assigned to analyzing-power data at those angles for which the actual statistical error was less than 1.5%. By using these different weightings for $\sigma(\theta)$ and $A_y(\theta)$, the $A_y(\theta)$ description was improved considerably

with almost no visible change in the fit to $\sigma(\theta)$; the latter result is expected from the low sensitivity of the differential cross section to the spin-orbit-potential parameters.

B. Deuteron elastic scattering from ^{206}Pb

Starting parameters for the optical-model searches were taken from the global set of Daehnick *et al.*[22] At first, the radial shape of the real potential was taken as the standard WS form, with components as prescribed in Ref. 22, and searches were made to obtain the best fit without restrictions on any of the parameters. However, the use of the best fit WS form of the potential (D1) produced analyzing powers at large angles that fell far below the measured values (not shown in Fig. 2). As a next step, an imaginary spin-orbit (ISO) term [see Eq. (2)] was added to the potential (WS+ISO), and an extensive 13-parameter search was made. This form of the potential gave a reasonably good fit to the analyzing-power data, although it still slightly underestimated these data at the largest angles, as seen from curve D2 in Fig. 2.

In order to investigate the influence of the radial shape of the potential form on the fit, it was changed from a WS form to a WS^2 form. This alteration did not produce any significant change in the quality of the fit compared to that of the WS form of the potential. However, when an imaginary spin-orbit term was added to the potential (WS^2+ISO), there was a dramatic improvement in the quality of fit for the analyzing-power data at large angles [see dashed-dot curve (D4) in Fig. 2].

The best-fit optical-model parameters obtained using various forms for the potentials are listed in Table II, while curves for these selected forms are shown in Fig. 2. With the exception of the potential sets D2 and D4, a common feature of all the other potential sets tried was a poor description of the analyzing-power data, particularly at the largest measured angles.

C. ^{3}He elastic scattering from ^{205}Tl

The parameters given by Hyakutake *et al.*[25] for ^{3}He elastic scattering from masses around $A=90$ were extrapolated to ^{205}Tl and taken as starting parameters. In addition, sets of parameters from Matsuoka *et al.*,[26] and Djaloeis *et al.*,[27] were also used as starting sets, although the latter have neither energy nor mass dependence. Taken together, these sets contain both "deep" and "shallow" family potentials with either volume or surface absorption. When searches were made, all the "shallow" family best-fit parameters converged to one final set of parameters, as was also the case for the "deep" family potentials. The resulting χ^2/point was about the same for both the shallow and deep potentials. Furthermore, the change in the radial shape of the real central potential from WS to WS^2 had negligible effect on the quality of fit to the data.

The list of best-fit optical-model parameters for ^{3}He elastic scattering from ^{205}Tl including the very recent global set (H0) of Trost *et al.*,[23] are listed in Table III. Figure 3 shows the resulting fits to the experimental data with the global set H0 and the best-fit parameter set H2.

TABLE II. Optical-model parameters for deuteron elastic scattering from ^{206}Pb at 79.4 MeV.

Set	Type	V (MeV)	r_0 (fm)	a_0 (fm)	W_S (MeV)	W_D (MeV)	r_w (fm)	a_w (fm)	V_{so} (MeV)	r_{so} (fm)	a_{so} (fm)	W_{so} (MeV)	r_{ws} (fm)	a_{ws} (fm)	r_c (fm)	J/A (MeV fm^3)	σ_r (mb)	χ^2/point
D0	WS (global)	80.09	1.170	0.844	6.67	7.60	1.325	0.929	2.52	1.070	0.660				1.30	313	3102	127
D1	WS	79.94	1.177	0.856	6.27	9.03	1.286	0.902	2.55	1.079	0.779				1.30	314	3006	46
D2	WS + ISO	80.67	1.174	0.861	5.93	9.52	1.298	0.846	2.59	1.072	0.712	−0.272	0.951	0.233	1.30	315	2947	19
D3	WS^2	87.38	1.317	0.625	7.05	7.66	1.282	0.990	2.92	1.062	0.791				1.30	306	3106	29
D4	WS^2 + ISO	85.76	1.326	0.609	6.36	8.50	1.268	0.972	2.72	1.062	0.714	−0.320	0.937	0.280	1.30	308	3061	10

IV. DISTORTED WAVE ANALYSES

Exact finite-range DWBA calculations were performed for all the observed transitions employing the computer code DWUCK5.[28] The distorted waves, in both entrance and exit channels, were generated using the optical-model parameters discussed in the previous section. The light-particle form factor[29] was obtained from a fit to electron-scattering data on ^{3}He at forward angles; only the S state of the ^{3}He wave function was used. The target form factor was generated by employing two distinct methods as discussed earlier and below. The spectroscopic strength G was extracted using the relation

$$\left[\frac{d\sigma}{d\Omega}\right]_{\text{expt}} = Gg\left[\frac{d\sigma}{d\Omega}\right]_{\text{DW5}}, \tag{5}$$

where $(d\sigma/d\Omega)_{\text{expt}}$ is the experimentally measured differential cross section, $(d\sigma/d\Omega)_{\text{DW5}}$ is the differential cross section predicted by the DWUCK5 code, and g is the light-particle spectroscopic strength which is here equal to 1.5. G is equal to C^2S, where C is an isospin Clebsch-Gordan coefficient, and S is the spectroscopic factor.

A. The target form factor

The target form factor, which contains the information about the nuclear structure, is generated by the WD method, where the depth of a Woods-Saxon potential is adjusted until the separation energy of the picked-up particle from the specified orbital is matched. For these calculations we chose the geometrical parameters of Streets, Brown, and Hodgson,[30] listed as set B1 in Table IV. The same parameters have also been used by Grabmayr *et al.*[8] in their study of the ^{208,206}Pb(d,^{3}He)^{207,205}Tl reactions.

Another approximation for calculating the form factor has been suggested by Austern[10] and Rae.[11] In this method, herein called the surface-peak (SP) method, a fixed mean-field potential plus an additional surface-peaked potential are used to describe the motion of the transferred nucleon. The depth of the additional surface-peaked potential is varied to match the separation energy of the transferred particle, thus ensuring the correct tail shape of the form factor. The surface-peaked potential can be interpreted as simulating the effects of the residual interaction at the nuclear surface. Of course, for closed-shell nuclei, the WD and SP methods yield the same results, since the SP potential term must then be zero. This SP method has been utilized in a study of the (^{9}Be,^{10}B) reaction by Winfield *et al.*,[12] where the strong absorption in both entrance and exit channels puts a premium on a reliable description of the bound state at the nuclear surface; more details can be found in Ref. 12. The potential parameters used in the present study for the calculation of the form factor by the SP method are listed as set B2 in Table IV; the geometrical parameters were obtained by the interpolation suggested in Ref. 30, wherein detailed analyses of the charge distribution of ^{40}Ca, and both matter and charge distributions of ^{208}Pb, have been carried out using a single-particle WS potential. The values of the poten-

TABLE III. Optical-model parameters for ^{3}He elastic scattering from ^{205}Tl at 78.4 MeV.

Set	Type	V (MeV)	r_0 (fm)	a_0 (fm)	W_S (MeV)	W_D (MeV)	r_w (fm)	a_w (fm)	r_c (fm)	J/A (MeV fm^3)	σ_r (mb)	χ^2/point
H0	WS (global)	151.85	1.150	0.864		28.83	1.206	0.800	1.40	374	2652	189
H1	WS (shallow)	126.71	1.185	0.785		27.37	1.209	0.881	1.30	331	2813	2.4
H2	WS (deep)	160.89	1.183	0.738		30.60	1.169	0.928	1.30	412	2970	2.5
H3	WS (shallow)	134.57	1.133	0.860	15.83		1.570	0.767	1.30	318	2823	3.4
H4	WS (deep)	178.38	1.102	0.846	17.20		1.556	0.787	1.30	389	2850	3.3
H5	WS^2	138.45	1.319	0.601		26.72	1.182	0.951	1.30	326	2903	3.1

TABLE IV. Bound state parameters[a] used in the present study.

Set	Method	V_0 (MeV)	V_{sur} (MeV)	r_0 (fm)	a_0 (fm)	V_{so}[b] (MeV)	r_{so} (fm)	a_{so} (fm)	r_c (fm)
B1	WD[c]	varied[d]	0.0	1.2675	0.810	6.00	1.10	0.65	1.20
B2	SP	fixed[e]	varied[f]	1.2670[g]	0.808[g]	5.35[h]	1.10	0.65	1.20

[a]No nonlocality is used for the bound state.
[b]$4V_{so}$ is used in DWUCK5.
[c]Geometrical parameters were taken from Ref. 30.
[d]Adjusted to match the separation energy of each state.
[e]The well depths V_0 were fixed at -60.39, -60.12, and -61.64 MeV, respectively, for the $3s_{1/2}$, $2d_{3/2-5/2}$, and $1h_{11/2}$ states.
[f]The surface-peaked potential was assumed to be of the derivative WS form and the depth of the surface peak was adjusted to match the separation energy of the state.
[g]The geometrical parameters for protons are calculated from Eq. (2.5) of Ref. 30. Note that the power $(-\frac{1}{3})$ for the masses is given incorrectly as $(+\frac{1}{3})$ in Ref. 30.
[h]Adjusted to give spin-orbit splitting between $2d_{3/2}$ and $2d_{5/2}$ levels in ^{208}Pb.

tial parameters for other nuclei are given by an interpolation formula [Eq. (2.5) of Ref. 30]. As the nucleus ^{206}Pb is very close to ^{208}Pb, the parameters obtained from the interpolation formula are considered reliable to describe the matter and charge distributions in ^{206}Pb. Also used in these calculations was a spin-orbit strength of 5.35 MeV, deduced from the splitting of the $2d_{5/2}$-$2d_{3/2}$ hole states in ^{207}Tl. Furthermore, following the suggestion of Millener and Hodgson,[31] the depths of the potentials for each orbit in the SP method were calculated to match the energy centroids previously determined from the spectroscopic strengths deduced with the WD method; these depths were -60.39, -60.12, and -61.64 MeV for the $3s_{1/2}$, $2d_{3/2-5/2}$, and $1h_{11/2}$ orbitals, respectively.

The rms radii of the nucleon orbitals (calculated at their energy centroids) obtained by the SP method are compared in Table V with the predictions from Hartree-Fock (HF) calculations of Brown *et al.*,[13] and of Decharge *et al.*[14] These rms radii for ^{206}Pb are in fact close to the values deduced for ^{208}Pb by Woods *et al.*[33] from a study of the sub-Coulomb (t,α) proton pickup reaction.

B. Choice of optical-model parameters

The sensitivity of the predicted DWBA cross sections and analyzing powers to the choice of the optical potentials in the entrance and exit channels was investigated. The bound-state parameters B1 in Table IV and the WD method have been used for this purpose. For the ^{206}Pb($\vec{d}$,^{3}He)^{205}Tl reaction at $E_d=79.4$ MeV, the matched angular momentum is about 4, and hence it is expected that the greatest sensitivity would be for the $l=0$ ($3s_{1/2}$) ground-state transition. This was indeed confirmed, as seen from Fig. 4, where comparisons are made for the entrance-exit parameter sets D2-H2, D4-H2, and D0-H0 from Tables II and III. Predictions of sets D1-H2 and D3-H2 are not shown in Fig. 4 as they were very similar in shape and magnitude to the sets D2-H2 and D4-H2, respectively. Similar calculations were also performed with set D2 in the entrance deuteron channel and sets H0, H1, H2, H3, H4, and H5 in the exit channel. In these cases the experimental shapes of the angular distributions of $\sigma(\theta)$ and $A_y(\theta)$ could not be accounted for with the "shallow" ^{3}He potential family, and the "deep" potential family gave considerably

TABLE V. rms radii[a] of proton orbitals in ^{206}Pb compared to Hartree-Fock predictions.

Orbital (nlj)	Present analysis	Brown *et al.*[b]	Decharge *et al.*[c]
$3s_{1/2}$	5.37	5.40	5.35
$2d_{3/2}$	5.51	5.53	5.46
$2d_{5/2}$	5.45	5.50	5.44
$1h_{11/2}$	6.06	6.13	6.09

[a]In units of fm.
[b]Reference 13.
[c]Reference 14.

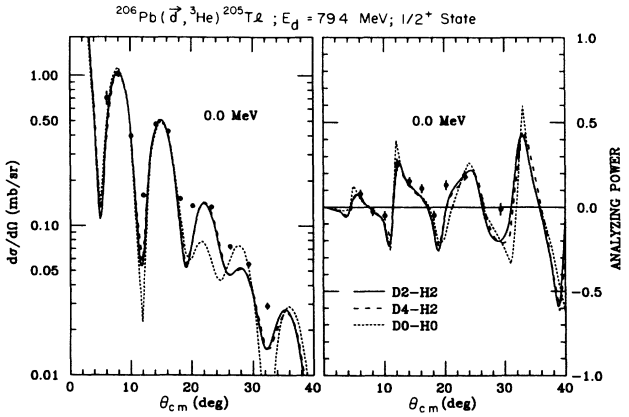

FIG. 4. Angular distributions of differential cross section and analyzing power for the $3s_{1/2}$ transition in the ^{206}Pb($\vec{d}$,^{3}He)^{205}Tl reaction at 79.4-MeV bombarding energy. The curves are the results of DWBA calculations using different sets of optical-model parameters described in the text.

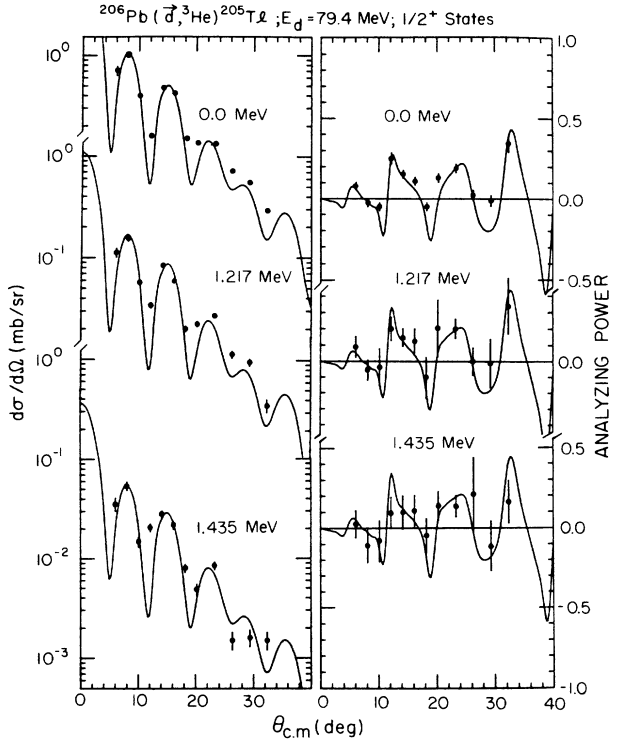

FIG. 5. Angular distributions of differential cross section and analyzing power for three $3s_{1/2}$ ($l=0$) transitions in the ^{206}Pb($\vec{d}$,^{3}He)^{205}Tl reaction at 79.4-MeV bombarding energy. The curves represent exact finite-range DWBA predictions with the SP method using the optical-model parameters D2-H2 and the standard nonlocality corrections given in the text.

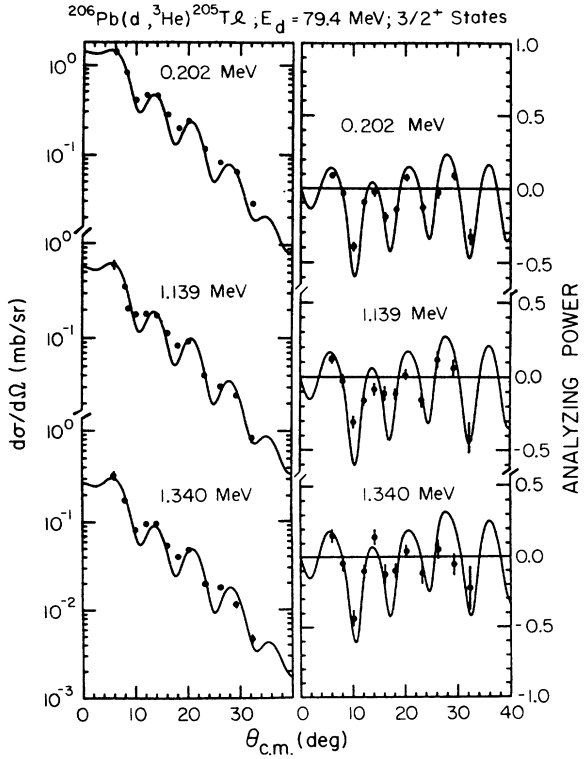

FIG. 6. Angular distributions of differential cross section and analyzing power for $2d_{3/2}$ ($l=2$) transitions. For further details see caption to Fig. 5.

better fits. Further, the use of volume-absorption potentials did not produce as good a fit as the surface absorption potentials. Based on all of these considerations, we finally chose the set D2 for deuterons in the entrance channel and set H2 for ^{3}He in the exit channel for the remainder of the calculations. The standard nonlocality corrections of $\beta=0.54$ and $\beta=0.25$ were used in all DWBA calculations for the deuteron and ^{3}He optical potentials, respectively.

V. RESULTS AND DISCUSSION

The DWBA predictions for angular distributions of the differential cross section and analyzing power for the ^{206}Pb($\vec{d}$,^{3}He)^{205}Tl reaction are shown in Figs. 5–9; these include proton pickup from the $3s_{1/2}$, $2d_{3/2}$, $2d_{5/2}$, and $1h_{11/2}$ orbitals. The angular distribution shapes are very well accounted for by the DWBA calculations. In particular, the agreement for $l=0$ transitions is good in spite of the fact that the matched orbital angular momentum is 4. The characteristic shapes of the analyzing powers for the $2d_{3/2}$ and $2d_{5/2}$ transitions are reproduced very well both in phase and magnitude.

Determination of the strengths for various configurations is an important goal of transfer-reaction

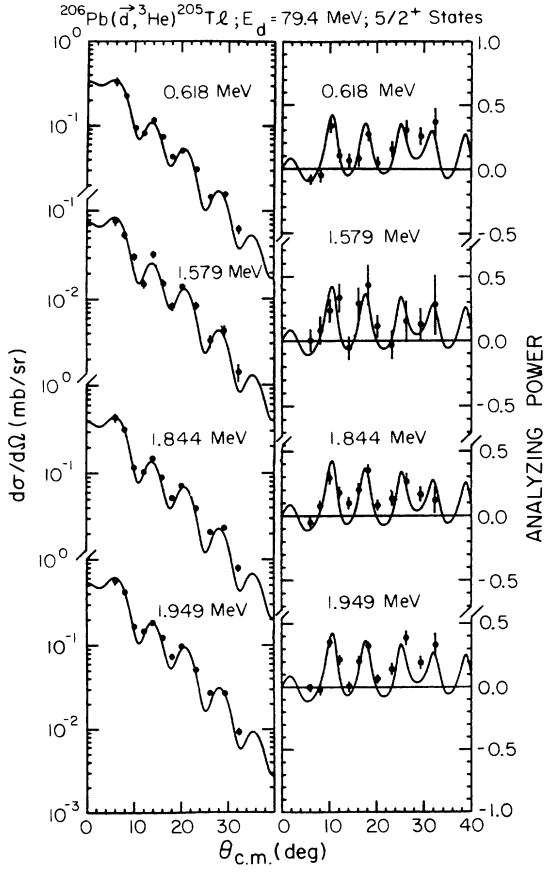

FIG. 7. Angular distributions of differential cross section and analyzing power for $2d_{5/2}$ ($l=2$) transitions. For further details see caption to Fig. 5.

studies to provide comparisons with detailed nuclear structure calculations. In this context both WD and SP methods were used in the present work to deduce the spectroscopic strengths for all 17 observed transitions by performing least squares fits to the data. In performing the least squares fits, greater weighting was given to the cross sections measured at the first observed peak. These spectroscopic strengths are listed in Table VI, where they are also compared with results from the $(\vec{t},\alpha)$ reaction[16] and various theoretical calculations.[34–36] Even though the SP and WD methods give roughly the same summed spectroscopic strengths, the actual values for individuals states differ by as much as 30% (e.g., the $\frac{5}{2}^+$ 0.618-MeV state).

The proton pickup strengths extracted in the present study with the SP method are 1.35 for the $3s_{1/2}$ orbital, 2.75 for the $2d_{3/2}$ orbital, 3.17 for the $2d_{5/2}$ orbital, and 8.45 for the $1h_{11/2}$ orbital. We assign an error of about 20% to these results (as discussed later, with particular attention to the $3s_{1/2}$ orbital), due to the uncertainties involved with the DWBA calculations and the absolute experimental cross sections. Compared to the simple shell-model sum rule values of 2, 4, 6, and 12, for the $3s_{1/2}$, $2d_{3/2}$, $2d_{5/2}$, and $1h_{11/2}$ orbitals, respectively, we observe a general quenching in the ^{206}Pb,(d,^{3}He)^{205}Tl reaction of about 30% for all orbitals with the exception of the $2d_{5/2}$ orbital, where we probably missed some strength lying at $E_x > 2.8$ MeV due to the small momentum acceptance of the QDDM magnetic spectrometer. In this regard it should be mentioned that Langevin-Joliot *et al.*[32] found using the near-isotope ^{208}Pb(d,^{3}He)^{207}Tl reaction at 108 MeV that the $2d_{5/2}$ strength is not concentrated only in the 1.67-MeV state in ^{207}Tl but is fragmented up to 8.3 MeV of excitation, the centroid being at 3.1 MeV. (Their results might similarly suggest that we may have missed a smaller amount of the $1h_{11/2}$ strength in our present study.) Therefore we believe it most likely that the extra missing $2d_{5/2}$ strength lies above our experimental acceptance, and is not due to a deficiency of the DWBA method, as the same method has been used for the $2d_{3/2}$ orbital in the present study.

The $3s_{1/2}$ strength obtained from the $(\vec{t},\alpha)$ reaction[16] is close to the shell-model limit, contrary to our results which indicate a 33% quenching of the strength. However, there is good agreement between our results and the $(\vec{t},\alpha)$ results for the $2d_{3/2}$ and $1h_{11/2}$ orbitals. The $(\vec{t},\alpha)$ strength for the $2d_{5/2}$ orbital is almost a factor of 2 less compared to our results, although the same transitions are seen in both reactions; the spectroscopic factors quoted from the $(\vec{t},\alpha)$ study have no errors assigned to

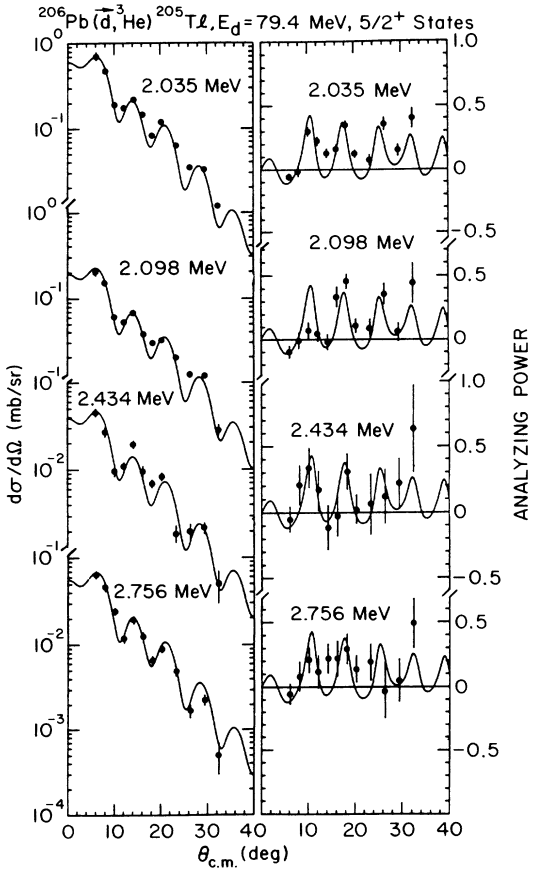

FIG. 8. Angular distributions of differential cross section and analyzing power for $2d_{5/2}$ ($l=2$) transitions. For further details see caption to Fig. 5.

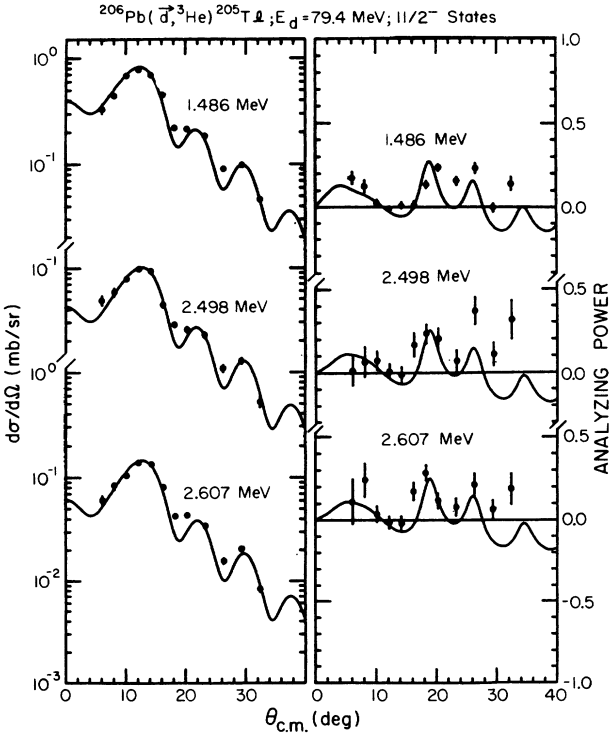

FIG. 9. Angular distributions of differential cross section and analyzing power for $1h_{11/2}$ ($l=5$) transitions. For further details see caption to Fig. 5.

them. These discrepancies may be due to "improper" handling of the form factor description in the DWBA analysis of the $(\vec{t},\alpha)$ reaction.

On the theoretical side, Azziz *et al.*[34] in their calculations with a core-coupling model assumed that the core states of ^{206}Pb are vibrational states, while Zamick *et al.*,[35] performed similar calculations (using the same model), but without assuming the core states of ^{206}Pb to be vibrational. Both calculations predict about the same strength for the $3s_{1/2}$ orbital. Results from the more explicit shell-model calculations of Silvestre-Brac and Boisson,[36] which have been performed using a basis that contains correlated pairs, are also listed in Table VI. In general, the predicted spectroscopic strengths are considerably larger than our experimental results, except for the $2d_{5/2}$ orbital where the predicted strength is too small. The latter might be due to partial inclusion of the $2d_{5/2}$ orbital in the configuration space of the shell-model calculations. Overall, predictions show a marginal depletion of the strength, mainly due to configuration mixing. Not taken into account in these calculations is a basic depletion due to short range and tensor correlations.[4,7]

The spectroscopic strengths for the $3s_{1/2}$ transitions, obtained from both the WD and SP methods in this study, are listed in Table VII, and are compared with other related experimental results. The errors quoted in Table VII include the following uncertainties combined in quadrature:

(i) 5% due to target thickness;
(ii) 5–15 % due to the fitting procedure;
(iii) 5% due to deuteron optical potentials;
(iv) 10% due to ^{3}He optical potentials;
(v) 5% due to the ^{3}He form factor;
(vi) 15% due to bound-state parameters;
(vii) 5–20 % due to least squares fit to the transfer-reaction data.

The errors in items (ii) and (vii) varied depending on the statistics of the data involved, while errors in items (iii) and (iv) were due to the difference in the DWBA predictions when different sets of optical-model parameters were used. Finally, we account for 15% error in item (vi) due to the target bound-state parameters which results from a change in the radius parameter r_0 by 1%

TABLE VI. Spectroscopic strengths G for the levels in ^{205}Tl.

E_x (MeV)	J^π	$(\vec{d},{}^3\text{He})$ 79.4 MeV[a] SP method	WD method	$(\vec{t},\alpha)$ reaction[b]	Theory Ref. 34	Ref. 35	Ref. 36
0.0	$\frac{1}{2}^+$	1.15	1.09	1.4	1.46	1.48	1.72
1.217	$\frac{1}{2}^+$	0.15	0.18	0.3	0.30		0.08
1.435	$\frac{1}{2}^+$	0.05	0.06	0.2			0.08
$\sum G(3s_{1/2})=$		1.35	1.33	1.9	1.76	1.48	1.88
0.202	$\frac{3}{2}^+$	1.77	1.61	1.6	2.08	2.36	2.64
1.139	$\frac{3}{2}^+$	0.66	0.74	0.8	0.40		0.76
1.340	$\frac{3}{2}^+$	0.32	0.37	0.4	1.16		0.08
$\sum G(2d_{3/2})=$		2.75	2.72	2.8	3.64	2.36	3.48
0.618	$\frac{5}{2}^+$	0.52	0.38	0.3[c]	0.60	0.60	0.48
1.579	$\frac{5}{2}^+$	0.11	0.10		0.12		0.48
1.844	$\frac{5}{2}^+$	0.55	0.54				0.96
1.949	$\frac{5}{2}^+$	0.75	0.74				
2.035	$\frac{5}{2}^+$	0.85	0.85				
2.098	$\frac{5}{2}^+$	0.27	0.28				
2.434	$\frac{5}{2}^+$	0.05	0.06				
2.756	$\frac{5}{2}^+$	0.08	0.09				
$\sum G(2d_{5/2})=$		3.17	3.04	1.8[d]	0.72	0.60	1.92
1.486	$\frac{11}{2}^-$	6.94	6.31	5.3[c]	8.40		9.36
2.498	$\frac{11}{2}^-$	0.62	0.94				
2.607	$\frac{11}{2}^-$	0.89	1.37				
$\sum G(1h_{11/2})=$		8.45	8.62	8.7[d]	8.40		9.36

[a]Present experiment.
[b]Reference 16.
[c]From Table 2 of Ref. 16.
[d]From Table 7 of Ref. 16.

TABLE VII. Spectroscopic strength for $3s_{1/2}$ proton pickup.

E_x (MeV)	$(\vec{d},{}^3He)$ at 79.4 MeV[a] SP method	WD method	(e,e'p) Expt.[b]	(d,^{3}He) at 52 MeV[c] WD method
0.0	1.15±0.22	1.09±0.22	1.10±0.05	1.42±0.29
1.22	0.15±0.05	0.18±0.05	0.20±0.02	0.22±0.05
1.44	0.05±0.03	0.06±0.03	0.08±0.01	0.07±0.02
$\sum G$	1.35±0.30	1.33±0.30	1.37±0.10	1.71±0.36

[a]Present experiment. Statistical and estimated systematic errors included as described in text.
[b]Reference 7. Errors are statistical, except ΣG, which includes 3% estimated systematic error.
[c]Calculated from results of Refs. 8 and 9. Statistical and estimated systematic errors included.

(which is about the uncertainty in r_0), both in the SP and WD methods.

Our results yield a $3s_{1/2}$ proton occupation number (from the SP method) $\sum G = 1.35$, in good agreement with the (e,e'p) results[6,7] of 1.37 (see Table VII). The results of the (e,e'p) experiment have an error of 11%, as compared to 20% from our results. This smaller error in (e,e'p) is mainly due to a reduced sensitivity of their results to the geometrical parameters used to calculate the bound-state wave function. Yet, it is important to note that the results of the (e,e'p) experiment are subject to change depending upon future changes in the value of z in Eq. (1). It is also significant that our $(\vec{d},{}^3He)$ experiment has an energy resolution about a factor of 2 superior to the (e,e'p) experiment, and the use of a polarized deuteron beam enabled us to assign definite spins and parities to the observed transitions without ambiguities. Based on all these observations we conclude that the study of the $(\vec{d},{}^3He)$ reaction is a reliable tool for probing nuclear structure provided one has all the necessary and correct ingredients to the DWBA analysis.

A value of $\sum G = 1.71$ was deduced from an earlier (d,^{3}He) study[9] at 52 MeV, with some efforts made to cancel out effects of uncertainties in the DWBA analysis by using ratios of the $3s_{1/2}$ spectroscopic factors for the ground state transitions of ^{206}Pb and ^{208}Pb. This result is larger than that obtained in the present analysis, and the (e,e'p) results of Refs. 6 and 7. It has been pointed out[6] that an explanation for this difference might reside in the geometry of the potential in which the $3s_{1/2}$ proton is bound in ^{206}Pb and ^{208}Pb. For example, in the WD analysis of the earlier (d,^{3}He) experiment,[9] if the potential radius r_0 is increased by 1% in ^{206}Pb with regard to ^{208}Pb, then good agreement is obtained with the (e,e'p) results.[6] However, such an arbitrary change in r_0 is inconsistent with the nuclear matter distributions[30] and would correspondingly drive the $\sum G$ obtained in the present work to low values, since the same bound-state geometry has been used in both (d,^{3}He) analyses. In any event, the results of all three experiments shown in Table VII are not in real disagreement considering the maximum error limits, although the authors of the earlier (d,^{3}He) work[8] do reach a different conclusion regarding the depletion of the $3s_{1/2}$ proton occupancy in ^{206}Pb relative to ^{208}Pb.

The occupation probabilities obtained from our experiment for all the orbitals in ^{206}Pb are compared in Table VIII with the corresponding experimental or predicted values in ^{208}Pb. The ratio $R = n(206)/n(208)$ indicates an additional depletion of about 20% due to configuration mixing in going from ^{208}Pb to ^{206}Pb. It is interesting to note that we observe the same general orbit (energy) dependence of the occupation numbers for ^{206}Pb as predicted for ^{208}Pb by Pandharipande *et al.*[4]

VI. CONCLUSIONS

A systematic study of the ^{206}Pb$(\vec{d},{}^3He)^{205}$Tl reaction has been made, including several steps taken to reduce uncertainties in the final results. Optical-model parameters used in the DWBA calculations for both entrance and exit channels were obtained from direct fitting of the measured elastic-scattering data, at the appropriate energies, thereby reducing uncertainties associated with the optical potentials. Exact finite-range DWBA calculations performed with a realistic ^{3}He form factor also reduced the uncertainty otherwise arising from the normalization constant required for zero-range DWBA. The angular distributions of both cross section and analyzing power are very well reproduced by the DWBA calculations even for the $l=0$ transitions which have a large angular-momentum mismatch at $E_d = 79.4$ MeV. The magnitude of the DWBA transfer cross section was found to be very sensitive to the bound-state radius parameter r_0 [by as much as $\Delta\sigma/\sigma \approx 12(\Delta r_0/r_0)$]. However, fixing the bound-state radius parameter value to charge and matter density distributions avoided large

TABLE VIII. Proton occupation probabilities in ^{206}Pb and ^{208}Pb.

Orbital (nlj)	$n(206)$[a]	$n(208)$
$3s_{1/2}$	0.67	0.82[b]
$2d_{3/2}$	0.69	0.83[c]
$2d_{5/2}$	0.53	0.90[c]
$1h_{11/2}$	0.70	0.90[c]

[a]Present experimental results (from SP method).
[b]Reference 7.
[c]Reference 4, but normalized to the value of 0.82 for the ground state. [The equation used is $n(e<e_F)=0.75-0.5x\ln x$, where $x = |e-e_F|/40$, and $e_F = -6.0$ MeV.]

uncertainties in the extracted spectroscopic factors. The bound-state parameters thus chosen in our calculations gave rms radii in good agreement with HF calculations and close to values for ^{208}Pb derived from a study of the sub-Coulomb (t,α) proton pickup reaction. The alternate "well-depth" and "surface peak" methods employed to generate the bound-state wave functions gave similar total spectroscopic strengths. For the orbitals studied, the major contribution to the overall uncertainty in the deduced spectroscopic strength came from the bound-state parameters.

Our final results show a 33% depletion of $3s_{1/2}$ proton strength in ^{206}Pb, in good agreement with (e,e'p) results. The extracted spectroscopic strength for the $2d_{3/2}$ and $1h_{11/2}$ orbitals was also observed to be quenched by about 30%. For the $2d_{5/2}$ orbital, some proton pickup strength might lie above $E_x = 2.8$ MeV, thus escaping detection in the present experiment. Furthermore, it appears that in going from the doubly magic nucleus ^{208}Pb to ^{206}Pb, there is an additional 20% quenching in the proton strength due to configuration mixing, over and above the basic depletion of 18% observed in ^{208}Pb due mostly to short-range correlations. In addition, the same orbit (energy) dependence of the occupation numbers for ^{206}Pb is observed as predicted by Pandharipande *et al.*[4] for ^{208}Pb.

Earlier theoretical calculations[34–36] predicted almost full occupancy of the $3s_{1/2}$ orbital, contradicting the present ($\vec{d}$,^{3}He) and recent (e,e'p) results. Perhaps more rigorous calculations are required which include the short-range and tensor correlations as in random-phase-approximation and nuclear matter calculations.

ACKNOWLEDGMENTS

We wish to thank P.D. Kunz for making available to us the ^{3}He form factor and also for numerous discussions. Thanks are also due to B.A. Brown and J. Decharge for making available to us the Hartree-Fock calculations. Discussions with M. H. Macfarlane and P.W.F. Alons are gratefully acknowledged. This work was supported in part by National Science Foundation Grants PHY81-14339 and 84-12177.

*Permanent address: Department of Physics, Bangalore University, Bangalore 560 001, India.

†Present address: Department of Physics, Princeton University, Princeton, NJ 08544.

[1] J. M. Cavedon, B. Frois, D. Goutte, M. Huet, Ph. Leconte, C. N. Papanicolas, X. H. Phan, S. K. Platchkov, and S. Williamson, Phys. Rev. Lett. **49**, 978 (1982).

[2] B. Frois, J. M. Cavedon, D. Goutte, M. Huet, Ph. Leconte, C. N. Papanicolas, X. H. Plan, S. K. Platchkov, and S. E. Williamson, Nucl. Phys. **A396**, 409c (1983).

[3] D. Gogny, in *Lecture Notes in Physics*, edited by H. Arenhovel and M. Danos (Springer-Verlag, Berlin, 1979), p. 88.

[4] V. R. Pandharipande, C. N. Papanicolas, and J. Wambach, Phys. Rev. Lett. **53**, 1133 (1984).

[5] M. Jaminon, C. Mahaux, and H. Ngo, Nucl. Phys. **A440**, 228 (1985).

[6] E. N. M. Quint, J. F. J. van den Brand, J. W. A. den Herder, E. Jans, P. H. M. Keizer, L. Lapikas, G. van der Steenhoven, P. K. A. de Witt Huberts, S. Klein, P. Grabmayr, G. J. Wagner, H. Nann, B. Frois, and D. Goutte, Phys. Rev. Lett. **57**, 186 (1986).

[7] E. N. M. Quint, B. M. Barnett, A. M. van den Berg, J. F. J. van den Brand, H. Clement, R. Ent, B. Frois, D. Goutte, P. Grabmayr, J. W. A. den Herder, E. Jans, G. J. Kramer, J. B. J. M. Lanen, L. Lapikas, H. Nann, G. van der Steenhoven, G. J. Wagner, and P. K. A. de Witt Huberts, Phys. Rev. Lett. **58**, 1088 (1987).

[8] P. Grabmayr, S. Klein, H. Clement, K. Reiner, W. Reuter, G. J. Wagner, and G. Seegert, Phys. Lett. **164B**, 15 (1985).

[9] H. Clement, P. Grabmayr, H. Röhm, and G. J. Wagner, Phys. Lett. **183B**, 127 (1987).

[10] N. Austern, Nucl. Phys. **A292**, 190 (1977).

[11] W. D. M. Rae, Ph.D. thesis, Oxford University, 1976 (unpublished).

[12] J. S. Winfield, N. A. Jelley, W. D. M. Rae, and C. L. Woods, Nucl. Phys. **A437**, 65 (1985).

[13] B. A. Brown, private communication.

[14] J. Decharge, private communication.

[15] S. Hinds, R. Middleton, J. H. Bjerregaard, Ole Hansen, and O. Nathan, Nucl. Phys. **83**, 17 (1966).

[16] E. R. Flynn, R. A. Hardekopf, J. D. Sherman, and J. W. Sunier, Nucl. Phys. **A279**, 394 (1977).

[17] W. R. Hering, H. Becker, C. A. Wiedner, and W. J. Thompson, Nucl. Phys. **A151**, 33 (1970).

[18] M. R. Schmorak, Nucl. Data Sheets **45**, 145 (1985).

[19] W. Haeberli, Annu. Rev. Nucl. Sci. **17**, 373 (1967).

[20] E. J. Stephenson, J. C. Collins, C. C. Foster, D. L. Friesel, W. W. Jacobs, W. P. Jones, M. D. Kaitchuck, P. Schwandt, and W. W. Daehnick, Phys. Rev. C **28**, 134 (1983).

[21] J. J. Kelly, University of Maryland, Program Manual, ALLFIT, 1983 (unpublished).

[22] W. W. Daehnick, J. D. Childs, and Z. Vrcelj, Phys. Rev. C **21**, 1127 (1980).

[23] H. J. Trost, P. Lezoch, and U. Strohbusch, Nucl. Phys. **A462**, 333 (1987).

[24] H. Leeb, General Optical Model Fitting Code, Atomic Institue of Austrian Universities, Vienna, 1984 (unpublished).

[25] M. Hyakutake, I. Kumabe, M. Fukada, T. Komatuzaki, T. Yamagata, M. Inoue, and H. Ogata, Nucl. Phys. **A333**, 1 (1980).

[26] N. Matsuoka, K. Hatanaka, M. Fujiwara, Y. Fujita, T. Saito, K. Hosono, A. Shimizu, M. Kondo, F. Ohtani, H. Sakaguchi, A. Goto, N. Nakanishi, and Y. Toba, Nucl. Phys. **A373**, 377 (1982).

[27] A. Djaloeis, J. P. Didelez, A. Galonsky, and W. Oelert, Nucl. Phys. **A306**, 34 (1978).

[28] P. D. Kunz, computer code DWUCK5, and extended as FRUCK2 by J. R. Comfort, Indiana University Cyclotron Facility Internal Report No. 85-1, 1985 (unpublished).

[29] P. D. Kunz, private communication.

[30] J. Streets, B. A. Brown, and P. E. Hodgson, J. Phys. G **8**, 839 (1982).

[31]D. J. Millener and P. E. Hodgson, Nucl. Phys. **A209**, 59 (1973).
[32]H. Langevin-Joliot, E. Gerlic, J. Guillot, and J. Van de Wiele, J. Phys. G **10**, 1435 (1984).
[33]P. W. Woods, R. Chapman, J. N. Mo, P. Skensved, and J. A. Kuehner, Phys. Lett. **116B**, 320 (1982).
[34]N. Azziz and A. Covello, Nucl. Phys. **A123**, 681 (1969).
[35]L. Zamick, V. Klemt, and J. Speth, Nucl. Phys. **A245**, 365 (1975).
[36]B. Silvestre-Brac and J. P. Boisson, Phys. Rev. C **24**, 717 (1981).